Soft Matter

ARTICLE TYPE

Millimeter-area, free standing, phospholipid bilayers[†]

Peter J. Beltramo,[a] Rob Van Hooghten,[b] and Jan Vermant[a*]

Minimal model biomembrane studies have the potential to unlock the fundamental mechanisms of cellular function that govern the processes upon which life relies. However, existing methods to fabricate free-standing model membranes currently have significant limitations. Bilayer sizes are often tens of micrometers, decoupling curvature or substrate effects, orthogonal control over tension, and solvent exchange combined with microscopy techniques is not possible, which restricts the studies that can be performed. Here, we describe a versatile platform to generate free standing, planar, phospholipid bilayers with millimeter scale areas. The technique relies on an adapted thin-film balance apparatus allowing for the dynamic control of the nucleation and growth of a planar black lipid membrane in the center of an orifice surrounded by microfluidic channels. Success is demonstrated using several different lipid types, including mixtures that show the same temperature dependent phase separation as existing protocols, moreover, membranes are highly stable. Two advantages unique to the proposed method are the dynamic control of the membrane tension and the possibility to make extremely large area membranes. We demonstrate this by showing how a block polymer, F68, used in drug delivery increases the membrane compliance. Together, the results demonstrate a new paradigm for studying the mechanics, structure, and function of model membranes.

1 Introduction

Model biomembrane systems have been extensively studied to elucidate fundamental biological processes, and as a result there are several routes to in vitro bilayer fabrication. Actively studied techniques include supported lipid bilayers (SLBs)[1–5], which provide excellent surface area for atomic force microscopy and fluorescence correlation spectroscopy, giant uni-lamellar vesicles (GUVs)[6–17], which are able to be manipulated by micro-pipettes and placed under tension, droplet-interface-bilayers (DIBs)[18–21], which facilitate the incorporation of membrane proteins and the detection of low-signal fluxes, and black lipid membranes (BLMs)[22–31], which are also suitable for electrical capacitance measurements of membrane protein activity. While each method has its strengths, each is appropriate for different studies and only duplicates certain characteristics of biological membranes. For example, membrane proteins are most easily incorporated in BLMs or DIBs, where the control over the membrane tension as in the GUV system or the large area present in SLBs is lacking.

In this paper, we present a platform to create large area model biomembranes (LAMBs) that incorporates the different capabilities of the existing methods into one technology to enable novel studies of membrane mechanics, structure, and function. The bilayers formed are free standing, able to be placed under tension, stable, and easily imaged by fluorescence microscopy due to their large area and planar geometry.

We focus on two test cases to demonstrate the capabilities of this platform: 1) lipid phase behavior in mixtures of saturated and unsaturated phospholipids fluidized by cholesterol and 2) controlled changes in membrane tension with the incorporation of block polymer in the aqueous phase. First, model lipid phase behavior has been studied since nanoscale heterogeneity in cell membranes, termed lipid rafts, is hypothesized to co-ordinate biological functions such as signaling, trafficking, and protein sorting[32]. In these studies, a mixture of high melting temperature lipid (1,2-dipalmitoyl-*sn*-glycero-3-phosphocholine, DPPC), a low melting temperature lipid (1,2-dioleoyl-*sn*-glycero-3-phosphocholine, DOPC), and cholesterol is shown to form a single phase at high temperatures. Upon decreasing the temperature the lipids laterally phase separate into domains visualized by fluorescence microscopy due to the exclusion of fluorophores from the more condensed phase. This allows for the measurement of domain diffusion to potentially extract the membrane viscosity[10,16,33] and examination of critical phenomena using the line tension between domains[34]. We show that the same miscibility

[a] Department of Materials, ETH Zürich, Vladimir-Prelog-Weg 5, 8093 Zürich, Switzerland. Fax: +41 44 632 11 78; Tel: +41 44 633 33 55; Email: jan.vermant@mat.ethz.ch

[b] Department of Chemical Engineering, KU Leuven, Celestijnenlaan 200F, 3001 Heverlee, Belgium.

transitions are detected with the LAMB technique, which allows for easy monitoring of domain boundaries due to the planar geometry. Second, the FDA-approved amphiphilic triblock polymer F68 (PEG_{40}-PPO_{27}-PEG_{40}) has been intriguing for its capability as a 'membrane sealant' to heal electropermeabilized cells [35,36] and as a possible treatment for Duchenne muscular dystrophy [37]. As a result, there have been some studies to elucidate the mechanism of its interaction with model monolayers [38–40], GUVs [41,42], and SLBs [43], with the holistic conclusion that the copolymer serves to alter the membrane tension and allow enhanced lipid fluidity to reseal membrane pores. We show how our platform can now be used to readily quantify the effect of F68 on changing the membrane tension, with implications for carrying out parametric studies to isolate and optimize the critical factors for possibly improved membrane sealant polymer design.

2 Results

To achieve large area, free standing, planar phospholipid bilayers, we use a modified thin film balance setup traditionally employed to study surfactant films in air [44–47]. The main operating principle relies on fine control of the disjoining pressure (to within 1 Pa) in the film balance cell by the use of a pressure transducer coupled with a PID controlled syringe (Fig. 1a). The bikewheel microchip consists of a 1 mm diameter central annulus (hub) with 24 microchannels extended radially (spokes) to connect with a larger channel (wheel). The microchip is glued onto a stainless steel holder/capillary which is placed inside an aluminum sample chamber for temperature control and attached to tubing for pressure control (Fig. 1b). The design of the chip has been modified from that originally developed by Pereira *et al.* [47] to ensure a fully axisymmetric film drainage in the central orifice by balancing the pressure drops (Fig. 1c). Lipids are dissolved in an oil phase at a concentration of 5 mg/mL and loaded into the microchip. Different oils, squalene and n-hexadecane, have been used with the same successful bilayer formation observed. The walls of the microchip are made hydrophobic to ensure the aqueous phase does not displace the lipid/oil mixture or wet the bikewheel channels as the film drains. An initially thick film of the lipid/oil mixture is surrounded by an aqueous buffer (150 mM NaCl, 2 mM $CaCl_2$, 0.2 mM $NaHCO_3$) to mimic physiological conditions (Fig. 1d). For stable bilayers, sufficient lipid must initially be present at the oil/aqueous interface. We have found the most success dissolving the lipids in the oil phase, with bilayer lifetimes much longer than necessary to perform experiments (greater than seven hours), however bilayers can still be formed by first dispersing lipids in the aqueous buffer. The aqueous compartments on the top and bottom of the film can be sealed off for independent solvent exchange or, in this study, connected so that a uniform hydrostatic pressure is imposed on the bilayer. From this initial state, the disjoining pressure across the film, which is defined as the difference between the pressure exerted on the film surface and that within the bulk film liquid [48], is increased slightly to initialize the controlled drainage of the thick film (Fig. 1d).

When the lipid/oil mixture thins to the molecular scale, interference patterns are observed by reflected light microscopy (Fig. 2a). Eventually, a black film nucleates and grows to form a cir-
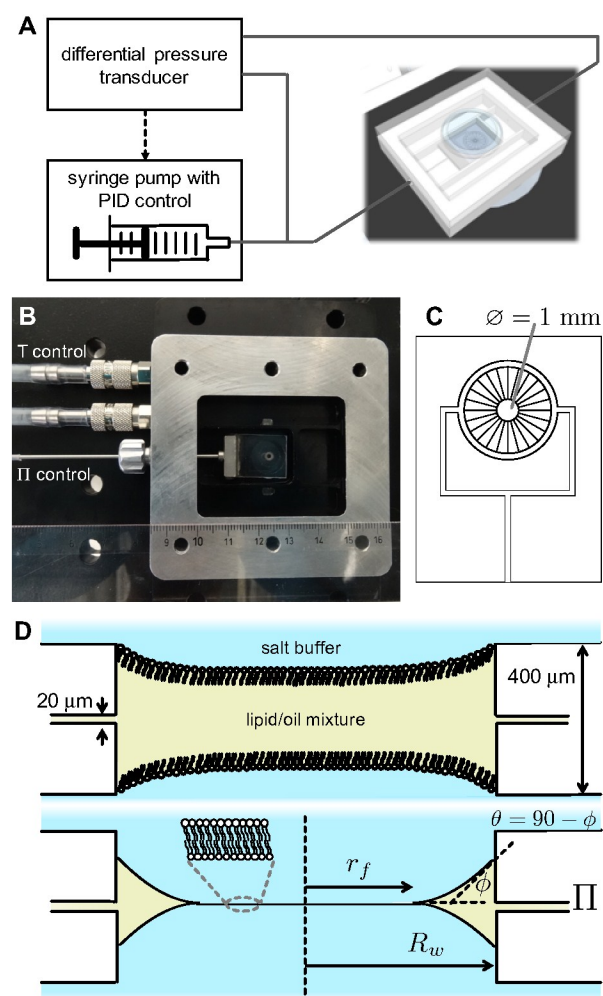

Fig. 1 LAMB platform schematics. (A) Experimental setup to create LAMBs, indicating the differential pressure transducer coupled with a syringe pump to measure and control the pressure within the thin film balance cell. (B) The microchip loaded within the thin film balance cell and tubing connections to pressure and temperature control. (C) Top view diagram of the bikewheel microchip channel geometry. The 1 mm diameter hole in the center allows the controlled drainage of liquid from the center hub through the microfluidic spoke channels. (D) Side view (not to scale) of an initially thick lipid film (top) draining in the center of the bikewheel microchannels due to increasing the disjoining pressure to eventually form a black lipid film (bottom). The membrane is stabilized by the outer annulus Plateau border, with the relevant parameters from the text indicated.

cular film in the center of the bikewheel orifice (Fig. 2b-f). The domain expansion kinetics are outside the scope of this paper, however we note that they empirically follow the same $A(t) \propto t$ dependence that is seen in surfactant thin films [49–51]. This circular film is stabilized by a liquid annulus of lipid/oil mixture. The radius of the film is also stable and can be controlled by changing the applied disjoining pressure. Unfortunately, the small change in refractive index between the oil/aqueous phase precludes the precise determination of the final film thickness by interferometry. The microscopy images in Fig. 2 show a monocomponent DOPC film forming from a DOPC/squalene mixture. Similar behavior is observed with n-hexadecane as the oil solvent and using a variety
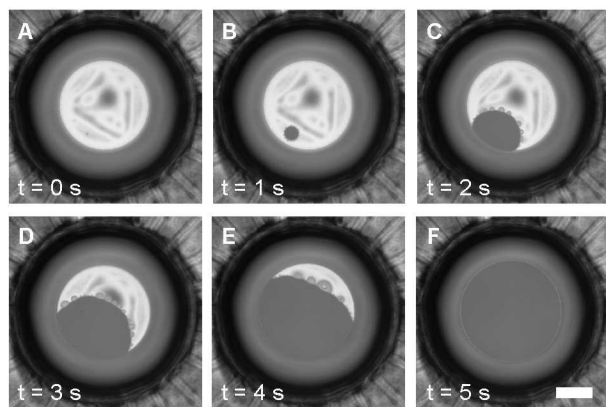
Fig. 2 Images of black lipid film formation from DOPC in squalene. (A) Interference fringes are observed as the oil thins. (B) Bilayer nucleation and (C-E) growth to eventually span the majority of the orifice radius (F). Frames are separated by 1 second and the scale bar represents 0.2 mm.
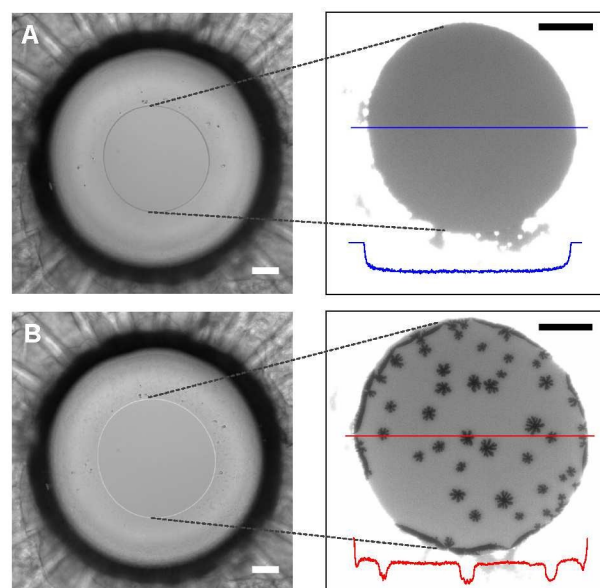

Fig. 3 Bilayer phase separation. Lipid domains appear when a film formed from a 34:33:33 molar ratio mixture of DOPC:DPPC:Chol at (A) 34°C is cooled to (B) 29°C (see also Supplementary Movie S1). Left panel is the imaging channel and the right panel is the fluorescence channel. Also shown is a linescan of the fluorescence signal which comes from the addition of 0.7 mol% Rh-DOPE that preferentially partitions into the more fluid phase. The scale bars represent 0.1 mm.

of lipids, including POPG, DPPC, DMPC, DOPG, E. coli total lipid extract, and lipid mixtures with cholesterol (see Supplementary Fig. S1-S8 and Movie S1-S5).

The phase behavior of the canonical 'lipid raft' mixture DOPC:DPPC:Chol has been studied extensively using giant unilamellar vesicles (GUVs)[9] because of its applicability to biologically relevant membranes. Here, we use it to validate successful bilayer formation in our device. An approximately equimolar mixture of DOPC:DPPC:Chol (with 0.7 mol% Rh-DOPE as a fluorescent lipid) formed at 34°C shows uniform fluorescence intensity across the bilayer (Fig. 3a). Upon cooling, dark domains nucleate at both the center and the edges of the bilayer, growing to form complex, acircular shapes (Fig. 3b and Supplementary Movie S1). It is well known that when undergoing miscibility transitions fluorescent lipids preferentially partition into the more fluid phase. The domains that form do not coalesce and maintain their acircular shape during the timescale of the experiment (hours). The fact that we observe a bimodal distribution of fluorescence intensities indicates that a single bilayer has formed. A multilamellar film or two monolayers separated by a thin layer of oil would result in more than two degrees of fluorescence intensity since the layers would not be in mechanical contact with one another. Furthermore, the temperature at which domains form in our system is within experimental error as that found in the GUV system[9,14] for different compositions of lipids, including the binary 60:40 mixture of DOPC and DPPC without cholesterol (Table 1, Supplementary Fig. S1-S2). A common challenge to reconstituting lipid mixtures into bilayers is guaranteeing that the bulk lipid composition is translated into the actual membrane composition. Although we do not have direct control over the composition in the bilayer and rely on molecules adsorbing to the interface in accordance with their bulk molar ratios, the congruence of our phase transition temperature data with published GUV results indicates that the phospholipid bilayers formed with this method have the same composition and are undergoing the same thermodynamic phase transitions.

Next, we show how the membrane tension of the planar bi-

Table 1 Temperature at which lipid domains first appear upon decreasing the temperature from a homogeneous bilayer.

| lipid molar ratio | transition T, °C | |
DOPC:DPPC:Chol	GUV	LAMB
34:33:33 (1:1:1)	29 ± 1[9]	30 ± 1
18:61:21 (1:2:1)	34 ± 1[9]	33.5 ± 1
60:40:0 (3:2:0)	27.3 ± 0.7[14]	27.7 ± 1

layer is controlled by the stabilizing disjoining pressure. We evaluate the membrane tension by applying Laplace's equation to the Plateau border that stabilizes the thin film[46],

$$\Pi = \frac{1}{r}\frac{\partial}{\partial r}\left[\frac{r\frac{\partial z}{\partial r}}{\left(1 + \left(\frac{\partial z}{\partial r}\right)^2\right)^{1/2}}\right]\sigma, \quad (1)$$

where σ is the membrane tension and Π is the disjoining pressure applied to the film, which is actively controlled and measured by the syringe pump/pressure transducer. Equation 1 is integrated twice with boundary conditions

$$\left.\frac{\partial z}{\partial r}\right|_{r=R_w} = \tan\phi \quad (2)$$

at the meniscus-chip interface, and

$$\left.\frac{\partial z}{\partial r}\right|_{r=r_f} = 0 \quad (3)$$

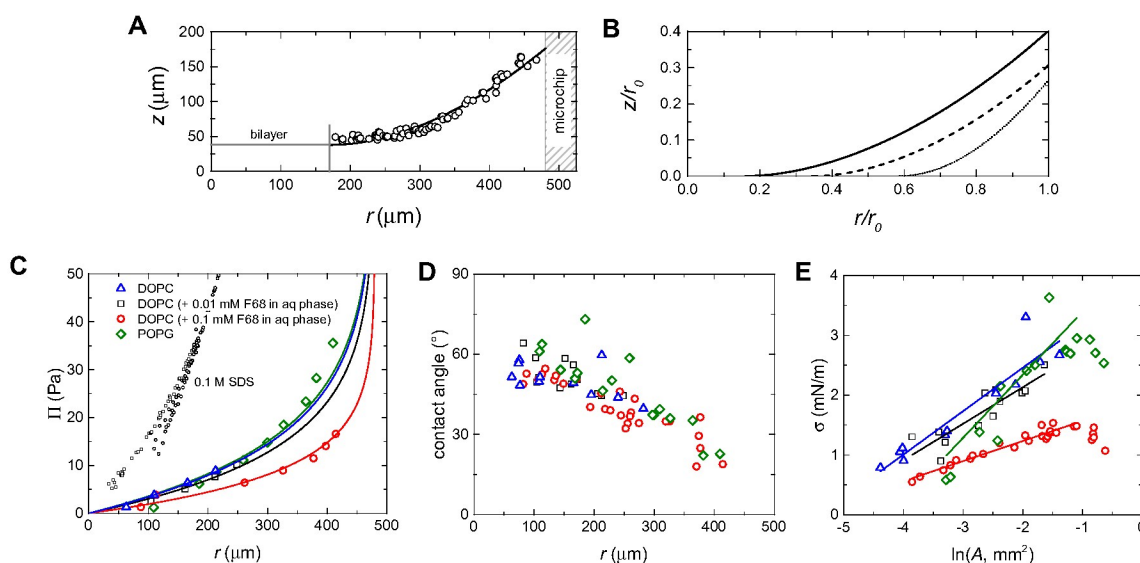at the bilayer-meniscus interface. This results in the following

Soft Matter Accepted Manuscript

Fig. 4 Measurement and control of membrane tension. (A) Exemplary height versus radial distance profile from confocal scans of fluorescent microspheres deposited on the oil/aqueous interface surrounding a DOPC bilayer. (B) The change in curvature of the Plateau border stabilizing the black lipid membrane for increasing DOPC membrane radii (from left to right: $\Pi = 2.6, 6.2, 13.1$ Pa and $r = 76, 166, 282$ μm). The radius of the bikewheel orifice, $r_0 = 480$ μm, is used to scale both axes. (C) There is a 60 Pa window in disjoining pressures which stabilize membranes with radii varying from the minimum to maximum possible within the microchip. For reference, this is orders of magnitude smaller than the maximum pressure able to maintain stability of typical surfactant black films in air, such as SDS, which are stable up to pressures of greater than 1000 Pa. (D) The contact angle decreases as the bilayer radius increases. (E) Linear relationship between membrane tension and the logarithm of the film area for different bilayers. For (C-E): DOPC membranes formed with aqueous phases with buffer only (blue triangles), buffer and 0.01 mM F68 (black squares) or buffer and 0.1 mM F68 (red circles) and POPG bilayers (green diamonds).

expression for the disjoining pressure,

$$\Pi = \frac{2\sigma R_w}{R_w^2 - r_f^2}\left(\frac{\tan\phi}{\sqrt{1-\tan^2\phi}}\right), \qquad (4)$$

where R_w is the bikewheel orifice radius, r_f is the bilayer radius, and $\theta = 90° - \phi$ is the meniscus-chip contact angle (Fig. 1c). The applied disjoining pressure versus radius relationship reveals a 50 Pa operating window over which the bilayer radius can be controlled, spanning areas from 0.007 mm^2 to 0.8 mm^2 (Fig. 4c). For comparison, using this setup an SDS film in air can be stabilized by electrostatic forces to disjoining pressures up to several thousand pascal. The fine pressure control achieved in the LAMB setup is mandatory for stable bilayers.

The meniscus-chip contact angle is sometimes assumed to be 90° in thin film balance studies of surfactant films in air, however we measure it directly. Fluorescent polystyrene spheres are gently micropipetted at the oil/aqueous phase interface to be used as a marker for the curvature of the Plateau border. The particles are irreversibly adsorbed to the interface and given the small values of the Bond number associated with the particle, we assume that deviations to the meniscus curvature due to the weight of the particles is negligible. A confocal scan is performed and the 3D particle locations are recorded[52], as well as the bilayer radius and location of the microchip. The corresponding particle height versus radial distance profile is used to determine the contact angle (Fig. 4a). Example profiles for a DOPC bilayer with increasing radius are shown in Fig. 4b. We observe that as the radius (disjoining pressure) increases, the height of the Plateau border and

contact angle at the microchip edge decreases (Fig. 4d). At small radii the contact angle is largest, $\sim 60°$, decreasing to $\sim 20°$ for the largest bilayers.

The experimentally applied disjoining pressure, measured bilayer radius, and measured meniscus contact angle data are given as input into Equation 4 to determine the membrane tension. From Fig. 4e, we see that as expected the membrane tension is a function of bilayer area, increasing from 0.5 mN/m to 3 mN/m. The headgroup characteristics and degree of saturation dictate the tension in monocomponent membranes, where differences are observed between DOPC and POPG. DOPC has an unsaturated carbon-carbon bond in each of its alkyl chains, while POPG has an unsaturated bond in only one of its alkyl chains. Additionally, the PG headgroup is anionic whereas PC is zwitterionic. The effect of incorporating the block polymer F68 in the aqueous phase buffer is also detected. As F68 concentration increases, the membrane tension decreases as well as the slope of the tension-area relationship.

In general, the membrane tension increases log-linearly with increasing bilayer area. The log-linear behavior suggests the definition of an elasticity modulus[53],

$$E = 2\frac{d\sigma}{d(\ln A)}, \qquad (5)$$

where A is the area of the membrane and a factor of two is used for the bilayer nature of the film. The previous equation is based on the observation that surfactant films behave as elastic membranes due to the increase of tension with area strain. It is im-

Table 2 Elasticity modulus of bilayers calculated from fitting Equation 5 to the membrane tension data of Fig. 4e.

Sample	E, mN/m
POPG	2.10 ± 0.62
DOPC	1.45 ± 0.18
DOPC (+ 0.01 mM F68)	1.22 ± 0.20
DOPC (+ 0.1 mM F68)	0.67 ± 0.04

portant to note that this value is different from the Gibbs elasticity, as measured for monolayers on a Langmuir trough, where it is assumed that the total number of molecules is constant over the course of the experiment, which is the case for insoluble surfactants or deformations that are fast compared to the adsorption/desorption timescale. The current experiment is performed in the opposite regime of very slow expansion, where the excess lipid concentration in the Plateau border is allowed to transfer into the film as the bilayer expands, so the number of lipids in the membrane and their area per molecule is not constant. Based on the fluorescence intensity change with slow area expansion/compression, the lipids in the membrane are more tightly packed at smaller areas (which agrees with the measurement of decreased tension), but we cannot quantify the lipid area per molecule over the course of these experiments, as yet. Nevertheless, larger values of the elasticity modulus indicate an increased resistance to deformation, while conversely lower values indicate increased compliance.

We determine the elasticity modulus of the membranes from a fit to Equation 5 and present the results in Table 2. The points at high membrane areas that deviate from the log-linear relationship are omitted from the fit. It is possible that at such large areas the curvature of the Plateau border becomes influenced by small heterogeneities in drainage due to the discrete locations of the microchannels, resulting in deviations from Equation 4.

3   Discussion

The elasticity modulus decreases from POPG to DOPC, likely due to decreased electrostatic repulsion between zwitterionic compared to anionic head groups. Importantly, the elasticity modulus of DOPC bilayers decreases with increasing F68 concentration in the aqueous phase. The cmc of F68 is 0.04 mM, and with a concentration below cmc the elasticity is marginally lowered. However, with 0.1 mM F68 the elasticity decreases by a factor of two compared to pure DOPC. This implies some degree of block polymer integration into the membrane to increase its compliance. Previous work on the effects of F68 on cell membranes suggest the block polymer integrates into the membrane, locally increasing lipid diffusion to seal membrane pores. Our results agree with that picture- here the bilayer increases compliance as F68 is added to the aqueous phase. We speculate that the hydrophobic block of F68 inserts into the membrane, and since it is larger than the phospholipids it is able to coil/uncoil to change its area as the bilayer is placed under strain to minimize changes in tension and increase compliance. There have been some molecular dynamics simulations evaluating the conformation of block polymers integrated with model membranes and its effect on membrane permeability[54,55]. While there are hints of altered membrane tension

(due to variations in lipid packing around the polymer) in one of the studies[55], the simulations are done under a tensionless state and the effect is not elaborated further. The experimental results here emphasize the importance of and clearly quantify the effect of block polymer integration on tension.

It is important to compare our results for membrane tension and domain formation to that reported using existing in vitro bilayer methodologies. In addition to physical characterization, controlling membrane tension has significant biological applications in understanding endocytosis[17] and lipid sorting[11]. The most common route to study bilayers under tension is by micropipette aspiration of GUVs[6]. For the GUV system, small changes in vesicle area correlate with a log-linear increase in membrane tension below values of 0.5 mN/m, which is used to calculate the bending (curvature) elastic modulus, while the behavior at higher tensions is used to calculate the areal stretch moduli. Specifically, for a DOPC GUV the bending moduli was determined to be 0.85×10^{-19} J using the low tension regime (< 0.5 mN/m) and the area stretch moduli was found to be 285 mN/m[7]. The tensions measured using the LAMB platform are in the latter regime, and are therefore a function of the extended, fluctuation-suppressed, conformation of the bilayer. The GUV experiment considers the compression of a tensed vesicle at a constant lipid concentration, and therefore can be considered an upper bound. The decreased moduli measured in our case is due to the non-constant lipid concentration within the bilayer, since as the membrane expands lipids may transfer from the bulk lipid/oil annulus to the bilayer to relieve the tension.

Notably, changing the membrane tension of a planar bilayer decouples the effects of curvature from the measurement, resulting in a deformation-independent quantification of the tension. The elastic properties of lipid bilayers are generally considered in the framework of the Helfrich Hamiltonian[56,57],

$$\mathscr{H}_0 = \int_A dS \left[\sigma + \frac{1}{2} \kappa_0 \left(c_1 + c_2 - 2c_0 \right)^2 + \bar{\kappa}_0 c_1 c_2 \right] \qquad (6)$$

where c_1 and c_2 are the local principle curvatures, c_0 is the spontaneous curvature, κ_0 is the bending modulus, and $\bar{\kappa}_0$ is the saddle splay modulus. The LAMB geometry facilitates independent interrogation of these parameters. Since the membrane is planar, c_1 and c_2 are initially zero and could potentially be controlled by applying a hydrostatic pressure across the membrane. Although symmetric bilayers ($c_0 = 0$) are studied in this work, spontaneous curvature effects can also be isolated and measured.

The membrane tension of BLMs has been measured using laser-induced surface deformation spectroscopy[31], applying a hydrostatic pressure difference across the bilayer[26] and by dynamic light scattering[23]. While the latter two methods give values in the $\sim$1 mN/m range, the bilayers measured using the first method are greater than $100\times$ less tense. These methods are all restricted to measuring as-formed BLMs, so the specific experimental protocol of bilayer formation and BLM aperture surface functionality may play a role in the membrane tension, and there is no control of it once the bilayer has formed. The current LAMB microchip surface functionality and pinning of the Plateau border allows the membrane tension to be modulated in the $\sim$1 mN/m range. With

additional fine-tuning of the pinning of the Plateau border, we anticipate lower tension membrane regimes can also be accessed with our platform.

While the temperature at which lipid domains appear is consistent between the LAMB technology and GUVs, we observe complex domain shapes, whereas circular domains form in GUVs. The domain shape in phase separated lipid mixtures is a competition between a variety of factors including the line tension between the two phases, membrane tension, cooling rate, phospholipid architecture, bending rigidities, and membrane curvature [58–60]. We suspect that the elimination of curvature in our planar membranes (with tension playing a secondary role) encourages the formation of complex rather than circular domain shapes. This result is not unusual, in fact binary DOPC/DPPC membranes phase separate into circular domains in GUVs [14] but form fractal domains in planar SLBs [61]. Certainly more work needs to be done to unequivocally separate the contributions of the different parameters to lipid phase separation and its consequences for lipid raft formation in cells.

The main drawbacks of BLM fabrication methods are that conventional BLM lifetimes are often less than two hours and the process to bilayer formation is not well controlled or reproducible, which constrains experiments [27]. It had previously been identified that the stability of the solvent annulus contributes to stability of films [25], leading BLM researchers to develop smaller microfabricated apertures [22] and/or tuning the aperture surface energy [29] to improve stability. The silanization process to prepare the LAMB microchips and the controlled drainage of the oil phase due to the pressure control scheme stabilizes the Plateau border pinning the membranes to result in bilayer lifetimes of at least seven hours. Additionally, we are not limited to the as formed bilayer since the tension can be controlled, solvent exchanged, and temperature modulated to give tremendous flexibility to the possible experiments.

Overcoming the membrane area limitations for a free standing, planar, bilayer has several advantages. If the device is complemented with patch-clamp type electronics to make electrical recordings of ion channels, the capacitance of the bilayer scales with membrane area, increasing signal to noise, and the collective functioning of many membrane channels could be measured. Large area membranes are also necessary for compatibility with scattering techniques to quantitatively measure the structure and fluctuations of the formed bilayers, and for ease of applying well defined deformation fields using active microrheological techniques or pressure gradients. Lastly, the size of the bilayer will increase the surface area available for mass transport across the membrane, and, coupled with control of the solvent conditions on either side of the membrane, this will facilitate precise measurement of chemical fluxes across the bilayer in combination with analytical techniques.

4 Conclusions

The LAMB technology presented here offers a versatile means to create large area model biomembranes from many lipids and lipid mixtures. The planar configuration facilitates experiments based on fluorescence microscopy, for example in the detection of lipid domains or rafts, particle microrheology, or fluorescent molecule adsorption and translocation. The free standing nature of the membrane allows independent access to both sides of the bilayer for the application of osmotic, thermal, chemical or hydrostatic pressure gradients. By using a microfluidic manifold with finely tuned surface chemistry, the pinning and controlled drainage of the oil-in-water film creates bilayers whose tension is manipulated, an obvious advantage for both fundamental bilayer mechanics and a means to detect the activity of mechanosensitive membrane protein channels in the future.

5 Methods

5.1 Materials

The phospholipids 1,2-dioleoyl-*sn*-glycero-3-phosphocholine (DOPC), 1,2-dipalmitoyl-*sn*-glycero-3-phosphocholine (DPPC), 1-palmitoyl-2-oleoyl-*sn*-glycero-3-phospho-(1'-*rac*-glycerol) (POPG), 1,2-dioleoyl-*sn*-glycero-3-phosphoethanolamine-N-(lissamine rhodamine B sulfonyl) ammonium salt (Rh-DOPE), 1,2-dioleoyl-*sn*-glycero-3-phosphoethanolamine-N-(7-nitro-2-1,3-benzoxadiazol-4-yl) ammonium salt (NBD-DOPE), 1,2-dioleoyl-*sn*-glycero-3-phospho-(1'-*rac*-glycerol) (DOPG), 1,2-dimyristoyl-*sn*-glycero-3-phosphocholine (DMPC), E. coli Total Lipid Extract, and cholesterol were obtained from Avanti Polar Lipids. Squalene, *n*-hexadecane, and octadecyltrichlorosilane (OTS) were purchased from Acros Organics. NaCl (99.99%, metals basis) and NaHCO$_3$ were obtained from Alfa Aesar. CaCl$_2$ was purchased from Sigma-Aldrich. The triblock polymer poly(ethylene glycol)$_{40}$-block-poly(propylene glycol)$_{27}$-block-poly(ethylene glycol)$_{40}$ (M$_n$ = 8400 g/mol) known as F68 or P188 was also purchased from Sigma-Aldrich. Yellow-green fluorescent polystyrene sulfate microspheres were purchased from Life Technologies ($2a = 1.0 \pm 0.013$ μm). All water used is ultra-pure water (Milli-Q, Merck-Millipore, resistivity $<$ 18.2 MΩ·cm).

5.2 Sample preparation

Lipid mixtures in chloroform are placed in a round-bottom flask and dried under a gentle stream of nitrogen. Any residual chloroform is removed by placing the sample under vacuum for at least one hour. Lipids are resuspended in oil (squalene or *n*-hexadecane) at a concentration of 5 mg/mL. The sample is bath-sonicated for at least two hours immediately after the addition of oil and also immediately before use to minimize lipid aggregates in the suspension. Lipid solutions are used within a week of preparation. A salt buffer of 150 mM NaCl, 2 mM CaCl$_2$, 0.2 mM NaHCO$_3$ and the desired concentration of F68 is prepared in ultra-pure water and filtered with a 0.2 μm pore filter to remove any particulates. For the confocal microscopy measurements, 10 μL of stock fluorescent polystyrene sphere suspension (2% solids) are diluted in 10 mL of the salt buffer for a final concentration of 0.1 % solids.

5.3 Microchip fabrication and preparation

Custom designed microfluidic bikewheel chips are fabricated by photolithography by Micronit Microfluidics. The channel design

is made by sequentially wet etching with HF the entrance and spoke channels onto a 0.7 mm by 15 mm by 20 mm glass borosilicate slide. The entrance channels and outer circular channel are 500 μm wide and 50 μm deep. The inner spoke channels are 45 μm wide and 20 μm deep, with a length of 0.8 mm. The etched slide is thermally bonded without intermediate layer to an identical borosilicate slide. To decrease the thickness of the chip where the film will form, the center of the chip is powder blasted on both sides to a depth of approximately 500 μm, leaving an inner taper thickness of 400 μm. A 1 mm diameter hole is drilled into the center of the microchip using a diamond drill. The chip is glued to a titanium holder using UHU two-component epoxy.

Before use the bikewheel microchips must be made hydrophobic. First, the chips are cleaned in a saturated solution of NaOH in ethanol in an ultrasonication bath for 20 minutes before being thoroughly rinsed with water. This removes any residual glass from drilling and/or organic contaminants in the channels and makes the glass saturated with silanol groups on the surface. Secondly, the chips are silanized by placement in 1 mM OTS in n-hexadecane for 24 hours. The chips are rinsed with n-hexadecane to remove unreacted OTS before being stored in water.

5.4 Experimental setup

The technique requires four main components: i) a differential pressure transducer (Baratron 120AD), ii) a syringe pump (Harvard Apparatus PHD Ultra CP), iii) a custom fabricated pressure chamber (either polyoxymethylene or aluminum for temperature control), and iv) the bikewheel microchip. The pressure chamber is designed with different compartments to allow independent control of the solution conditions on either side of the bilayer. Tubing connects the measurement side of the pressure transducer, syringe pump, and microchip. The bidirectional differential pressure transducer has a $\pm$ 10 torr (1333 Pa) range with 0.0001 torr (0.01333 Pa) resolution. The transducer is coupled to the syringe pump, which runs a PID control loop in a computer interface to control the applied disjoining pressure within 1 Pa. The pressure chamber can either be sealed, with the reference side of the transducer connected to the air within the cell, or left unsealed, with the reference side of the transducer open to the atmosphere.

The microchip is first loaded with the lipid/oil mixture, taking care to eliminate any air bubbles in the channels as these hinder pressure measurement, before inserting it into the chamber and connecting the measurement side tubing. Aqueous buffer is then gently added to the chamber. A thick film of lipid/oil is formed within the bikewheel annulus and allowed to drain slowly. After interference fringes appear in the thin oil layer, the nucleation and growth of a black lipid film is observed, whose diameter is then controlled by the applied disjoining pressure. For temperature dependent measurements, the lipid/oil mixture, aqueous buffer, and pressure chamber are preheated before following the above procedure.

For observing bilayer formation and measuring lipid domain appearance, the sample is imaged on an upright microscope (Nikon Eclipse FN1) with a 10x long working distance objective and a Hamamatsu ORCA-Flash4.0 CMOS camera. A tri-band filter allows simultaneous imaging using λ = 505 nm for reflection and λ = 555 nm for fluorescence. For measuring the curvature of the Plateau border, the sample is imaged on a confocal microscope (Nikon Eclipse Ti-E with a VT-Infinity3 confocal scan head) with a 10x long working distance objective and a Hamamatsu C9100 CCD camera. In this case, the fluorescent polystyrene microspheres are gently pipetted to the oil/water interface while the thick film is present, before thinning and bilayer formation. A 200 μm z-scan is carried out with Δz = 0.2 μm, 20 ms exposure time, 15 μm pinhole aperture and appropriate barrier filter/dichroic for λ = 515 nm excitation.
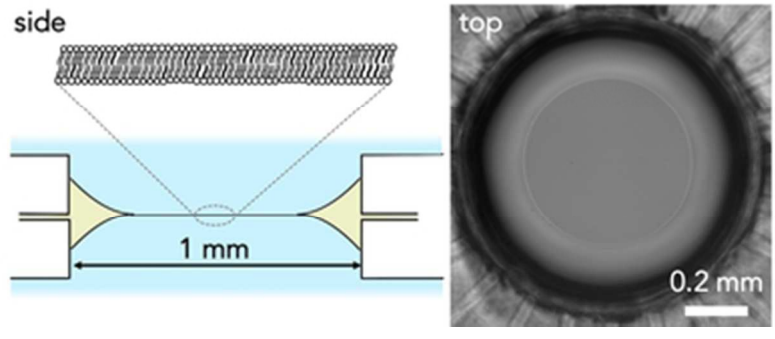
6 Acknowledgements

References

1 E. T. Castellana and P. S. Cremer, *Surface Science Reports*, 2006, **61**, 429–444.

2 L. Zhang and S. Granick, *P. Natl. Acad. Sci. U.S.A.*, 2005, **102**, 9118–9121.

3 M.-P. Mingeot-Leclercq, M. Deleu, R. Brasseur and Y. F. Dufrêne, *Nature Protocols*, 2008, **3**, 1654–1659.

4 P. Kukura, H. Ewers, C. Müller, A. Renn, A. Helenius and V. Sandoghdar, *Nature Methods*, 2009, **6**, 923–927.

5 A. Hemmerle, L. Malaquin, T. Charitat, S. Lecuyer, G. Fragneto and J. Daillant, *P. Natl. Acad. Sci. U.S.A.*, 2012, **109**, 19938–19942.

6 E. Evans and W. Rawicz, *Phys. Rev. Lett.*, 1990, **64**, 2094–2097.

7 W. Rawicz, K. C. Olbrich, T. McIntosh, D. Needham and E. Evans, *Biophys. J.*, 2000, **79**, 328–339.

8 T. Baumgart, S. T. Hess and W. W. Webb, *Nature*, 2003, **425**, 821–824.

9 S. L. Veatch and S. L. Keller, *Biophys. J.*, 2003, **85**, 3074–3083.

10 P. Cicuta, S. L. Keller and S. L. Veatch, *J. Phys. Chem. B*, 2007, **111**, 3328–3331.

11 B. Sorre, A. Callan Jones, J.-B. Manneville, P. Nassoy, J.-F. Joanny, J. Prost, B. Goud and P. Bassereau, *P. Natl. Acad. Sci. U.S.A.*, 2009, **106**, 5622–5626.

12 R. Dimova, N. Bezlyepkina, M. D. Jordö, R. L. Knorr, K. A. Riske, M. Staykova, P. M. Vlahovska, T. Yamamoto, P. Yang and R. Lipowsky, *Soft Matter*, 2009, **5**, 3201–3212.

13 M. Dezi, A. Di Cicco, P. Bassereau and D. Lévy, *P. Natl. Acad. Sci. U.S.A.*, 2013, **110**, 7276–7281.

14 D. Chen and M. M. Santore, *Biochimica et Biophysica Acta (BBA) - Biomembranes*, 2014, **1838**, 2788–2797.

15 F. Quemeneur, J. K. Sigurdsson, M. Renner, P. J. Atzberger, P. Bassereau and D. Lacoste, *P. Natl. Acad. Sci. U.S.A.*, 2014, **111**, 5083–5087.

16 T. T. Hormel, M. A. Reyer and R. Parthasarathy, *Biophys. J.*, 2015, **109**, 732–736.

17 Z. Shi and T. Baumgart, *Nature Communications*, 2015, **6**, 5974.

18 H. Bayley, B. Cronin, A. Heron, M. A. Holden, W. L. Hwang, R. Syeda, J. Thompson and M. Wallace, *Mol. BioSyst.*, 2008, **4**, 1191–1208.

19 A. Fischer, M. A. Holden, B. L. Pentelute and R. J. Collier, *P. Natl. Acad. Sci. U.S.A.*, 2011, **108**, 16577–16581.

20 S. Leptihn, O. K. Castell, B. Cronin, E.-H. Lee, L. C. M. Gross, D. P. Marshall, J. R. Thompson, M. Holden and M. I. Wallace, *Nature Protocols*, 2013, **8**, 1048–1057.

21 G. de Wit, J. S. H. Danial, P. Kukura and M. I. Wallace, *P. Natl. Acad. Sci. U.S.A.*, 2015, **112**, 12299–12303.

22 R. S. Ries, H. Choi, R. Blunck, F. Bezanilla and J. R. Heath, *J. Phys. Chem. B*, 2004, **108**, 16040–16049.

23 M. F. Hildenbrand and T. M. Bayerl, *Biophys. J.*, 2005, **88**, 3360–3367.

24 P. V. Ganesan and S. G. Boxer, *P. Natl. Acad. Sci. U.S.A.*, 2009, **106**, 5627–5632.

25 T.-J. Jeon, N. Malmstadt, J. L. Poulos and J. J. Schmidt, *Biointerphases*, 2008, **3**, FA96.

26 A. D. Petelska, *Cent. Eur. J. Chem.*, 2011, **10**, 16–26.

27 M. Khan, N. Dosoky and J. Williams, *International Journal of Molecular Sciences 2013, Vol. 14, Pages 21561-21597*, 2013, **14**, 21561–21597.

28 P. Kongsuphol, K. B. Fang and Z. Ding, *Sensors and Actuators B: Chemical*, 2013, **185**, 530–542.

29 L. K. Bright, C. A. Baker, M. T. Agasid, L. Ma and C. A. Aspinwall, *ACS Appl. Mater. Interfaces,* 2013, **5**, 11918–11926.

30 J. Geng, K. Kim, J. Zhang, A. Escalada, R. Tunuguntla, L. R. Comolli, F. I. Allen, A. V. Shnyrova, K. R. Cho, D. Munoz, Y. M. Wang, C. P. Grigoropoulos, C. M. Ajo-Franklin, V. A. Frolov and A. Noy, *Nature*, 2014, **514**, 612–615.

31 T. Takei, T. Yaguchi, T. Fujii, T. Nomoto, T. Toyota and M. Fujinami, *Soft Matter*, 2015, **11**, 8641–8647.

32 D. Lingwood and K. Simons, *Science*, 2009, **327**, 46–50.

33 C. A. Stanich, A. R. Honerkamp-Smith, G. G. Putzel, C. S. Warth, A. K. Lamprecht, P. Mandal, E. Mann, T.-A. D. Hua and S. L. Keller, *Biophys. J.*, 2013, **105**, 444–454.

34 A. R. Honerkamp-Smith, P. Cicuta, M. D. Collins, S. L. Veatch, M. den Nijs, M. Schick and S. L. Keller, *Biophys. J.*, 2008, **95**, 236–246.

35 R. C. Lee, L. P. River, F. S. Pan, L. Ji and R. L. Wollmann, *P. Natl. Acad. Sci. U.S.A.*, 1992, **89**, 4524–4528.

36 J. M. Collins, F. Despa and R. C. Lee, *Biochimica et Biophysica Acta (BBA) - Biomembranes*, 2007, **1768**, 1238–1246.

37 S. Yasuda, D. Townsend, D. E. Michele, E. G. Favre, S. M. Day and J. M. Metzger, *Nature*, 2005, **436**, 1025–1029.

38 G. Wu, J. Majewski, C. Ege, K. Kjaer, M. J. Weygand and K. Y. C. Lee, *Phys. Rev. Lett.*, 2004, **93**, 028101.

39 S. A. Maskarinec, J. Hannig, R. C. Lee and K. Y. C. Lee, *Biophys. J.*, 2002, **82**, 1453–1459.

40 K. Kita-Tokarczyk, F. Itel, M. Grzelakowski, S. Egli, P. Rossbach and W. Meier, *Langmuir*, 2009, **25**, 9847–9856.

41 J.-Y. Wang, J. Chin, J. D. Marks and K. Y. C. Lee, *Langmuir*, 2010, **26**, 12953–12961.

42 C.-Y. Cheng, J.-Y. Wang, R. Kausik, K. Y. C. Lee and S. Han, *Biomacromolecules*, 2012, **13**, 2624–2633.

43 J. Wang, L. Segatori and S. L. Biswal, *Soft Matter*, 2014, **10**, 6417–6424.

44 A. Sheludko and D. Exerowa, *Kolloid Z*, 1959, **165**, 148–151.

45 K. J. Mysels and M. N. Jones, *Discussions of the Faraday Society*, 1966, **42**, 42–50.

46 P. M. Claesson, T. Ederth, V. Bergeron and M. W. Rutland, *Adv Colloid Interfac*, 1996, **67**, 119–183.

47 L. Pereira, C. Johansson, H. W. Blanch and C. J. Radke, *Colloids Surf., A*, 2001, **186**, 103–111.

48 B. V. Derjaguin, N. V. Churaev and V. M. Muller, *Surface Forces*, Springer US, Boston, MA, 1987, pp. 25–52.

49 P. A. Kralchevsky, A. Nikolov, D. T. Wasan and I. Ivanov, *Langmuir*, 1990, **6**, 1180–1189.

50 P. Heinig, C. Márquez-Beltrán and D. Langevin, *Phys Rev E*, 2006, **73**, 051607.

51 Y. Zhang and V. Sharma, *Soft Matter*, 2015, **11**, 4408–4417.

52 Y. Gao and M. L. Kilfoil, *Opt. Express*, 2009, **17**, 4685.

53 K. J. Mysels, M. C. Cox and J. D. Skewis, *J. Phys. Chem.-Us*, 1961, **65**, 1107–1111.

54 S. Hezaveh, S. Samanta, A. De Nicola, G. Milano and D. Roccatano, *J. Phys. Chem. B*, 2012, **116**, 14333–14345.

55 S. Nawaz, M. Redhead, G. Mantovani, C. Alexander, C. Bosquillon and P. Carbone, *Soft Matter*, 2012, **8**, 6744–6754.

56 F. L. H. Brown, *Annu. Rev. Phys. Chem.*, 2008, **59**, 685–712.

57 P. Bassereau, B. Sorre and A. Lévy, *Adv Colloid Interfac*, 2014, **208**, 47–57.

58 J. Hu, T. Weikl and R. Lipowsky, *Soft Matter*, 2011, **7**, 6092–6102.

59 J. J. Amazon, S. L. Goh and G. W. Feigenson, *Phys Rev E*, 2013, **87**, 022708.

60 B. Palmieri, T. Yamamoto, R. C. Brewster and S. A. Safran, *Adv Colloid Interfac*, 2014, **208**, 58–65.

61 U. Bernchou, J. Brewer, H. S. Midtiby, J. H. Ipsen, L. A. Bagatolli and A. C. Simonsen, *J Am Chem Soc*, 2009, **131**, 14130–14131.

33x13mm (300 x 300 DPI)